Available online at www.sciencedirect.com

ScienceDirect

Advances in Space Research 67 (2021) 749–761

ADVANCES IN SPACE RESEARCH (a COSPAR publication)

www.elsevier.com/locate/asr

# Simulation study of motion of charged particles trapped in Earth's magnetosphere

Pankaj K. Soni *, Bharati Kakad, Amar Kakad

*Indian Institute of Geomagnetism, New Panvel (West), Navi Mumbai, India*

Received 18 July 2020; received in revised form 11 October 2020; accepted 15 October 2020
Available online 30 October 2020

**Abstract**

This article aims to understand the motion of the charged particles trapped in the Earth's inner magnetosphere. The emphasis is on identifying the numerical scheme, which is appropriate to characterize the trajectories of the charged particles of different energies that enter the Earth's magnetosphere and get trap along the magnetic field lines. These particles perform three different periodic motions, namely: gyration, bounce, and azimuthal drift. However, often, the gyration of the particle is ignored, and only the guiding center of the particle is traced to reduce the computational time. It is because the simulation of all three motions (gyro, bounce, and drift) together needed a robust numerical scheme, which has less numerical dissipation. We have developed a three-dimensional test particle simulation model in which the relativistic equation of motion is solved numerically using the fourth and sixth-order Runge-Kutta methods. The stability of the simulation model is verified by checking the conservation of total kinetic energy and adiabatic invariants linked with each type of motion. We found that the sixth-order Runge-Kutta method is suitable to trace the complete trajectories of both proton and electron of a wide energy range, 5 keV to 250 MeV for $L = 2–6$. We have estimated the bounce and drift periods from the simulations, and they are found to be in good agreement with the theory. The study implies that a simulation model with sixth-order Runge-Kutta method can be applied to the time-vary, non-analytical form of magnetic configuration in future studies to understand the dynamics of charged particles trapped in Earth's magnetosphere.


*Keywords:* Test particle simulation; Trapped particle trajectories; Adiabatic invariants; Runge-Kutta method; Earth's inner magnetosphere

## 1. Introduction

The Earth's magnetic field can be approximated by the dipolar magnetic field in the inner magnetosphere up to $6R_e$ (Baumjohann and Treumann, 2012). The charged particles trapped in the Earth's inner magnetosphere perform three types of periodic motions. They gyrate around magnetic field lines, bounce over magnetic mirror points, and azimuthally drift around the Earth (Williams, 1971). Energies of these trapped particles range from $\sim$ eV to $\sim$ 100 MeV. In the order of low to high energies, they are prevalent in the plasmasphere ($\sim$ eV), ring current ($\sim$1–100 keV), and radiation belts ($\geqslant$100 keV) region (Ebihara and Miyoshi, 2011; Millan and Baker, 2012). These particles undergo different physical processes, and their flux and energies are highly variable, even on geomagnetically quiet periods. This is due to variations in the solar wind conditions and their interaction with different plasma waves that are excited through various plasma instabilities in the Earth's inner magnetosphere. The presence of higher energy (keV-MeV) particles in the Earth's magnetosphere, especially in the radiation belts, has been reported through satellite observations (Millan and Baker, 2012; Mozer et al., 2013; Reeves et al., 2013). The solar wind particles

* Corresponding author.
*E-mail addresses:* pankajs123321@gmail.com (P.K. Soni), bharati.kakad@iigm.res.in (B. Kakad), amar.kakad@iigm.res.in (A. Kakad).

https://doi.org/10.1016/j.asr.2020.10.020
0273-1177/

enter Earth's magnetosphere with low energies (~10–100 eV) (Bittencourt, 2011), and their interaction with waves can accelerate them to higher energies (~ MeV), which contributes significantly to the dynamics of the radiation belt (Elkington et al., 2003; Engel et al., 2015; Hudson et al., 2017; Katoh and Omura, 2004; Ozaki et al., 2019; Tobita and Omura, 2018). Despite different energies, the motion of these charged particles is governed by the Earth's magnetic field. They are trapped in the Earth's inner magnetosphere until they fall into the loss cone and get lost into the upper atmosphere Yugo and Iyemori (2001).

In the past, several studies have been carried out to understand the dynamics of these magnetospheric charged particles. Hones and Edward (1963) conducted a theoretical analysis to investigate the motions of charged particles trapped in the distorted magnetosphere. They have calculated drift paths for the particles whose motion is confined to the magnetic equatorial plane, and mirroring particles at low altitudes. Delcourt et al. (1990) used three-dimensional particle code for ions to examine the motion of near-Earth plasma-sheet particle during substorm. Ukhorskiy and Sitnov (2008) analyzed the radial transport of electrons due to ULF fluctuations in the inner magnetosphere using the test particle approach under the guiding center approximation. Sorathia et al. (2018) studied the evolution of the outer radiation belt during the geomagnetic storm using test particle and magnetohydrodynamic (MHD) simulations. However, the guiding center of the particle is traced in most of the magnetospheric simulation to reduce the computational time. It is because the simulation of all three motions (gyro, bounce, and drift) together needed a robust numerical scheme, which has less numerical dissipation.

Similarly, Öztürk (2012) performed test particle simulation to investigate particle motion in the dipolar magnetic field using the fourth-order Runge-Kutta method and demonstrated gyro, bounce, and drift motion for proton. However, the fourth-order Runge-Kutta method is limited to trace the trajectory of proton of energy 10 MeV up to one drift only. When the simulation is carried out for the lower energy protons, drift motion results are numerically unstable. Moreover, the electron is 1836 times less massive than the proton, making the electron gyro-period three order smaller than the proton. This suggests the need for a smaller time step to simulate the electron trajectories, which ultimately becomes computationally expensive. Therefore, the fourth-order Runge-Kutta method can not be used to validate theoretically calculated bounce periods of electron and drift periods of both electron and proton. It invokes the need for an efficient numerical scheme capable of simulating gyro, bounce, and drift motions of the charged particles in the Earth's magnetosphere. Thus, in the present simulation model, we aim to examine the appropriate numerical scheme applicable to characterize the trapped particles (both electrons and protons) dynamics and produce physically valid simulation results.

We have considered a static dipolar configuration for the Earth's magnetic field, with no inhomogeneities. The equation of motion is solved numerically by both fourth and sixth-order Runge-Kutta methods. In the simulation model, the particle can perform gyration, bounce, and drift motions self-consistently. The performance of the simulation model and numerical schemes is tested by verifying the conservation of total kinetic energy and adiabatic invariants associated with each type of motion. We found that the sixth-order Runge-Kutta method is efficient in simulating both electrons and proton's trajectories for a wide range of energy and L-shell. There can be many circumstances in the Earth's magnetosphere where adiabatic invariants itself are not conserved (Antonova and Kropotkin, 2003; Birmingham et al., 1967; Mukherjee and Rajaram, 1981). Such physical processes are not incorporated in the present simulation.

This paper is structured as follows. The model equations and the numerical schemes used in the simulation are given in Section 2. In Section 3, the numerical stability of the numerical schemes used in the simulation model is verified. The application of this model is presented in Section 4. The results are discussed in Section 5 and concluded in Section 6. In Appendix A, B, and C, we have respectively briefed the Runge-Kutta numerical scheme, derivations of the theoretical equations of the bounce, and the drift periods of trapped particles.

## 2. Model equations and numerical schemes

We have used a test particle approach in which the plasma is considered as a single particle system, and its effect on the ambient parameters is neglected. This is a reasonable approximation to understand the dynamics of trapped particles in the Earth's inner magnetosphere. The relativistic equation of motion for a particle of charge $q$ and mass $m$, under the action of the Lorentz force due to magnetic field, $\mathbf{B}$ can be written as,

$$\gamma m_0 \frac{d\boldsymbol{v}}{dt} = q\boldsymbol{v} \times \boldsymbol{B}(\boldsymbol{r}). \tag{1}$$

The position of charged particle can be computed from the velocity using following expression,

$$\boldsymbol{v} = \frac{d\boldsymbol{r}}{dt}. \tag{2}$$

Here, $\gamma = (1 - v^2/c^2)^{-1/2}$ is the relativistic factor, $m = \gamma m_0$ and $\boldsymbol{v} = [v_x, v_y, v_z]$ is the velocity vector. The magnitude of velocity is estimated from the kinetic energy, $E_k$ using the following expression,

$$v = c\sqrt{1 - \left(\frac{m_0 c^2}{m_0 c^2 + E_k}\right)^2}. \tag{3}$$

If the magnetic field is constant, the particle's acceleration will be perpendicular to the magnetic field, and it will gyrate around the magnetic field line. The particles under

such motion will have an instantaneous gyro-frequency, $\Omega = q \mid \mathbf{B} \mid /\gamma m_0$ and gyro-radius, $\rho = \gamma m_0 v_\perp / q \mid \mathbf{B} \mid$, depending on the perpendicular velocity ($\boldsymbol{v}_\perp$) and magnetic field $\mathbf{B}$. In the present study, we have considered the ambient magnetic field to be dipolar for the Earth's inner magnetosphere, where the magnetic field lines are closed. In this region, the terrestrial magnetic field $\mathbf{B}(\mathbf{r})$ can be expressed in the Cartesian coordinate system as (Griffiths, 2005),

$$\mathbf{B}(\mathbf{r}) = -\frac{B_0 R_e^3}{r^5}[3xz\hat{\mathbf{x}} + 3yz\hat{\mathbf{y}} + (2z^2 - x^2 - y^2)\hat{\mathbf{z}}]. \quad (4)$$

Here, horizontal $xy$-plane is the magnetic equator and z-axis is the vertical magnetic axis, which is illustrated in Fig. 1. At the magnetic equator on the surface of Earth, the magnetic field strength is measured to be $B_0 \approx 3.07 \times 10^{-5}$ T. In the simulation code, Eqs. (1) and (2) are solved numerically from fourth (RK4) and sixth (RK6) order Runge-Kutta methods. The expressions for the RK4 and RK6 schemes (Luther, 1968; Portero et al., 2012) are respectively given as,

$$v_x^{t+\Delta t} = v_x^t + \frac{\Delta t}{6}[k_1 + 2k_2 + 2k_3 + k_4], \quad (5)$$

$$v_x^{t+\Delta t} = v_x^t + \frac{\Delta t}{5}\left[\frac{16k_1}{27} + \frac{6656k_3}{2565} + + \frac{28561k_4}{11286} - \frac{9k_5}{10} + \frac{2k_6}{11}\right] \quad (6)$$

After discretizing Eqs. (1) and (2), we get six equations which gives rate of change of $v_x, v_y, v_z, x, y$ and $z$. At the initial time $t = 0$, the corresponding values of velocity and position components are $[vsin(\alpha_{eq})cos(\psi), vsin(\alpha_{eq})sin(\psi), vcos(\alpha_{eq})]$ and $[x, 0, 0]$. Here $\alpha_{eq}$ is the equatorial pitch angle, the angle between the velocity vector of a particle and the total magnetic field at the magnetic equator. The $\psi$ is gyro-phase, which can vary from 0 to $2\pi$ and decides the particle entry in the horizontal $xy$-plane. For all simulation runs, we have taken fixed $\psi = 0^\circ$ and $\alpha_{eq} = 30^\circ$. We took initial position as $[x = L, 0, 0]$ by varying $L$ between 2 and 6. In Eqs. (5) and (6), $v_x^{t+\Delta t}$ is the Runge-Kutta approximation of $v_x$ at time $[t + \Delta t]$, which is determined by the present value $v_x^t$ plus the weighted average of all increments from $k_1$ to $k_6$. The details of these two numerical schemes are given in Appendix A. The size of time interval, $\Delta t$ is taken as $\sim 1/50$ times of the gyro-period. In the same way, one can compute $v_y, v_z, x, y, z$. In this model, first we compute the velocity components $[v_x, v_y, v_z]$, and then utilize these estimates to compute the position components $[x, y, z]$.

As an example, the trajectory of a proton with energy $E_k = 5$ MeV at $L = 4$ obtained from the simulation code having sixth-order Runge-Kutta scheme is shown in Fig. 2 for 120 s. Here, Fig. 2a shows the three-dimensional motion of proton, whereas the top view of its trajectory, as seen from the north magnetic pole, is depicted in Fig. 2b. The motion is helical around the magnetic field lines. The magnetic field's gradient and curvature introduce two additional motions: the bounce and the drift motion. The motion due to the parallel component of velocity is the bounce motion, which is the periodic north-south oscillation along the magnetic field lines. As the particle moves towards the stronger magnetic field's location, it reflects from the mirror point due to the mirror force. The gradient in the magnetic field is responsible for the drift in the direction perpendicular to both $\nabla B$ and $\mathbf{B}$ (Chen, 1984). The drift motion takes the particle in the azimuthal direction, perpendicular to the bounce motion and across the magnetic field lines. The frequency of the bounce motion is smaller than the gyro-motion and higher than the drift motion. The shown trajectory of the proton can also be validated from Fig. 2 of Öztürk (2012) since both the studies have approximated Earth's inner magnetosphere as a dipolar configuration. However, the numerical schemes used to simulate the particle dynamics are different (RK4 and RK6).

In the similar manner, the trajectory of electron of energy $E_k = 5$ MeV, and $L = 4$ is shown in Fig. 3 for 120 s. It may be noted that unlike proton (see Fig. 2), the gyro motion of the electron is not distinctly visible in Fig. 3. The electron has a very small gyro-radius, so it gyrates very close to the magnetic field lines. The electron drifts slowly as compared to the proton; hence it shows less azimuthal coverage in Fig. 3 compared to the proton in

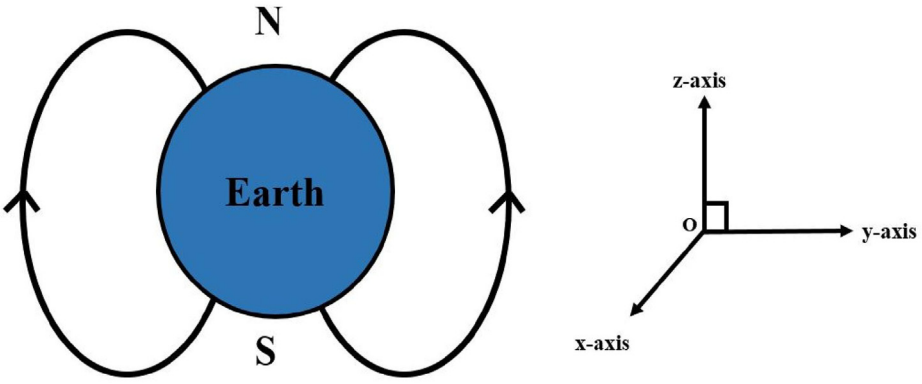


Fig. 1. Illustration of the magnetic field lines of the Earth, represented as a dipole magnetic field directed from the magnetic south to north direction. The horizontal $xy$-plane is the magnetic equatorial plane with z-axis as vertical magnetic axis. Here, we have used the magnetic coordinate system assuming Earth's magnetic field to be dipolar.

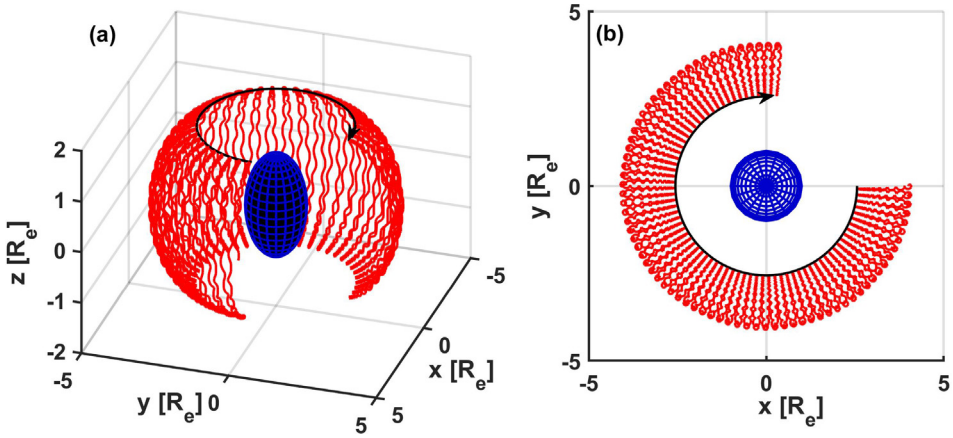


Fig. 2. The trajectories of proton of energy 5 MeV at $L = 4$ with pitch angle of $\alpha_{eq} = 30^{\circ}$ in Earth's dipolar magnetic field for 120 s. The dipole moment is in $-\hat{z}$ direction. The black arrows show westward motion of proton due to $\nabla B \times \boldsymbol{B}$ drift. (a) shows three-dimensional trajectory of proton (b) the top view of the proton motion in $xy$ plane as seen from the north magnetic pole.

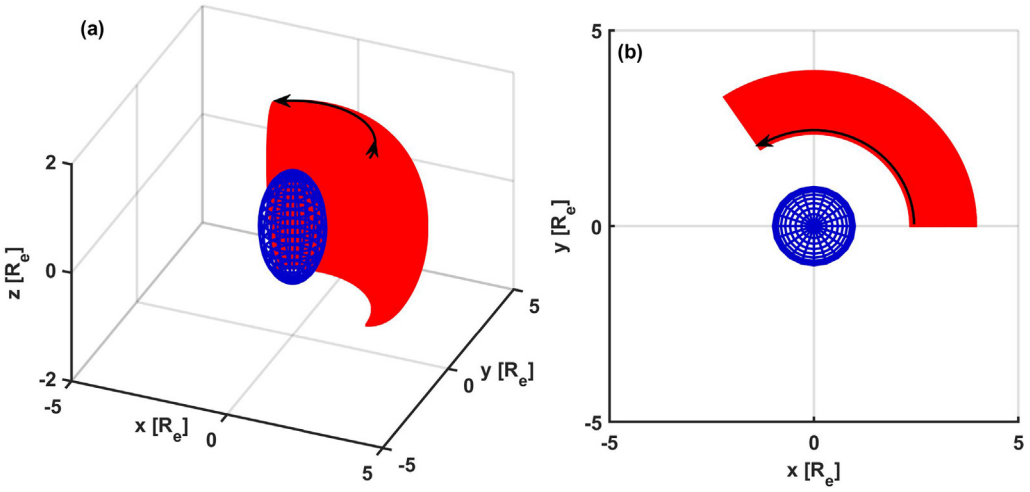


Fig. 3. The trajectories of electron of energy 5 MeV at $L = 4$ with pitch angle of $\alpha_{eq} = 30^{\circ}$ in Earth's dipolar magnetic field for 120 s. The dipole moment is in $-\hat{z}$ direction. The black arrows show eastward motion of electron due to $\nabla B \times \boldsymbol{B}$ drift. (a) shows three-dimensional trajectory of electron (b) the top view of the electron motion in $xy$ plane as seen from the north magnetic pole.

120 s. In this way, the particles in the dipolar magnetic field are trapped on closed drift shells as long as they are not disturbed by collisions or interactions with plasma waves to fall into the loss cone and get lost into the upper atmosphere. To estimate the bounce and drift periods, we transformed position $[x, y, z]$ to $[r, \lambda, \phi]$ using the following equations.

$$\begin{aligned} r &= \sqrt{x^2 + y^2 + z^2}, \\ \lambda &= sin^{-1}(\tfrac{z}{r}), \\ \phi &= cos^{-1}(\tfrac{x}{rsin\lambda}). \end{aligned} \tag{7}$$

The time variation of these transformed spherical coordinates $[r, \lambda, \phi]$ are depicted in Fig. 4 for proton of energy $E_k = 5$ MeV, and $L = 4$. The simulation employed with the sixth-order Runge-Kutta method is used to get these details. Here, **r** represents the radial distance of particles from the center of the Earth. $\lambda$ represents magnetic latitude, which varies between $-90^{\circ}$ to $+90^{\circ}$. The variation of $\lambda$ with time can be used to calculate the time taken by particle to complete one bounce period. $\phi$ is the azimuthal angle, which varies from $0^{\circ}$ to $360^{\circ}$ over one complete drift. It is used to estimate the drift period of the charged particle. This way, we have used the simulation model to trace trajectories of charged particles having different energies, and $L$-shells in the Earth's inner magnetosphere. For the data shown in Figs. 2–4, we have used the simulation model having sixth-order Runge-Kutta method. The reason for preferring sixth-order over fourth-order Runge-Kutta numerical scheme is discussed in the next section.

## 3. Validation of numerical scheme

In the present simulation study, we have used the fourth and sixth-order Runge-Kutta methods to solve the

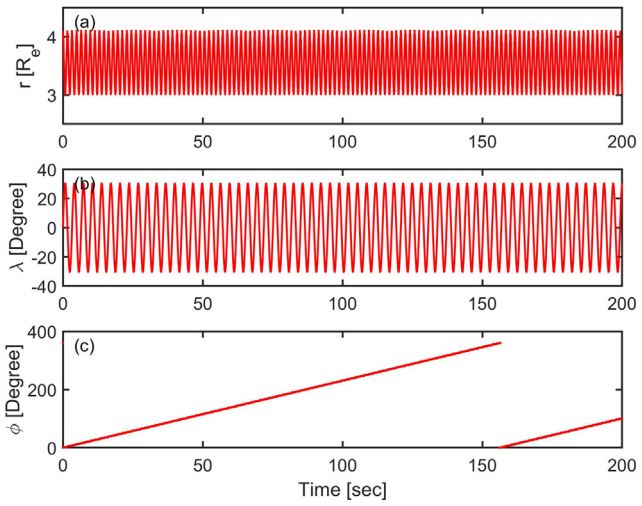


Fig. 4. The spherical coordinates associated with the trajectory of proton of energy 5 MeV at $L = 4$, which is trapped in the Earth's dipolar field. **r** is the radial distance of the trapped particle from the center of the Earth in terms of Earth's radius. The periodic time variation of $\lambda$ (magnetic latitude) represents the bounce motion. The maximum and minimum value of $\lambda$ corresponds to the magnetic mirror points in the northern and southern hemispheres, respectively. The variation of $\phi$ represents the change in azimuthal angle over the drift motion.

equation of motion. The suitability of these numerical schemes to trace the charged particle's complete trajectory is verified in this section. Using these numerical schemes, we have simulated the trajectories of both proton and electron of energy 5 MeV at $L = 4$. The time variation of the particle's kinetic energy normalized w.r.t. its initial kinetic energy, $E_k/E_{k0}$, and magnetic latitude obtained from the simulation using sixth-order (blue) and fourth-order (red) Runge-Kutta methods are shown in Fig. 5 for proton (Fig. 5a, c) and electron (Fig. 5b, d).

We noticed that the sixth-order Runge-Kutta method reduces the numerical error considerably so that there is negligible numerical dissipation. It maintains a constant $E_k/E_{k0}$, which implies that the system's energy is conserved. The particle bounces back and forth from the same magnetic latitude representing the periodic orbit for an arbitrarily long simulation time. On the other hand, when the fourth-order Runge-Kutta method is used, the ratio $E_k/E_{k0}$ continuously decreases with time, which implies a faster increase in the numerical error. It may also be noted that, for this case, the magnetic latitudes of the mirror points are not the same during the bounce motion of the particle. If we compare simulation outputs for proton and electron, i.e., Fig. 5a with 5b, and 5c with 5d, we find that the numerical error enhances rapidly for electron as compared to the proton. It suggests that numerical dissipation in the fourth-order Runge-Kutta method is considerably higher, and it increases within the first few seconds of the simulation run. It may be noted that the $\Delta t$ for proton is $10^{-4}$ s, and for electron, it is $10^{-7}$ s. Thus, in 300 s

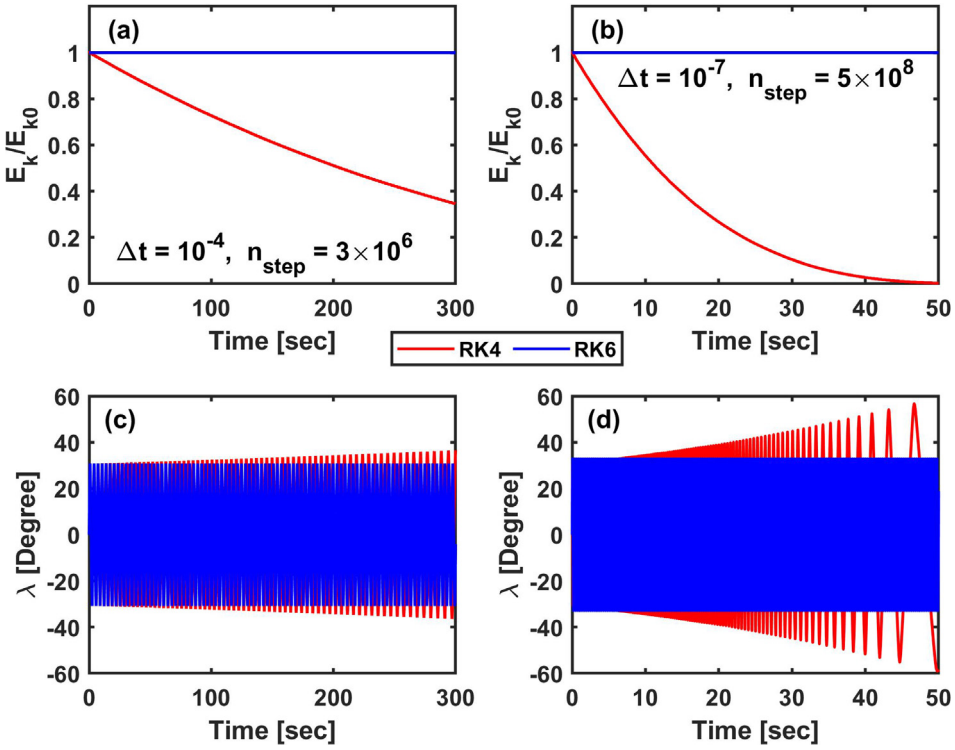


Fig. 5. (a-b) Ratio of kinetic energy of the particle at each time step to its initial kinetic energy ($E_k/E_{k0}$) and (c-d) magnetic latitude ($\lambda$) as a function of time obtained from the simulation model having fourth-order (red) and sixth-order (blue) Runge-Kutta methods for proton and electron. Here $E_{k0} = 5$ MeV is the initial energy of proton and electron placed at $L = 4$ with equatorial pitch angle 30°. The sixth-order Runge-Kutta method shows fairly good long-term conservation of kinetic energy and stable mirror point locations due to less numerical dissipation unlike the fourth-order Runge-Kutta method. (For interpretation of the references to color in this figure legend, the reader is referred to the web version of this article.)

and 50 s of the simulation run, the velocity and position of proton and electron are computed for $3 \times 10^6$ and $5 \times 10^8$ number of time steps, respectively. In each computation step, the numerical error gets integrated. Hence, in the case of electron, where the number of computation time steps, $n_{step}$ are more, the numerical error increases faster as compared to the proton. Therefore, the fourth-order Runge-Kutta method can not simulate the electron and proton drift motion in the Earth's inner magnetosphere.

Furthermore, we examined the conservation of adiabatic invariants during proton and electron motions in the simulation. For the particles in the dipolar magnetic field, adiabatic invariants ($J_1$,$J_2$, and $J_3$) are associated with gyration, bounce, and drift motion, respectively (Kellogg, 1959; Northrop and Teller, 1960; Walt, 2005). Each invariant can be obtained from the closed line integral of the particle's canonical moment over one cycle of the associated motion. The first adiabatic invariant is associated with the gyro-motion and can be written as,

$$J_1 = \langle \frac{\pi \gamma^2 m_0^2 v_\perp^2}{q \mid B \mid} \rangle. \tag{8}$$

The first adiabatic invariant explains the existence of mirror points. As the particle moves towards the polar region, where the ambient magnetic field is stronger, its perpendicular velocity increases, and parallel velocity decreases to keep $J_1$ and $E_k$ constant. At a particular point, its parallel velocity becomes zero, and the particle bounces back. The first adiabatic invariants estimated from the simulation using both the numerical schemes are shown in Fig. 6(a) for the proton of energy 5 MeV at $L = 4$. In Fig. 6(a), the blue and red color curves respectively represent the non-averaged component of the first adiabatic invariant obtained from the sixth- and fourth-order Runge-Kutta method. The black line shows their averaged component, i.e., $J_1$. Here, non-averaged $J_1$ oscillates with the local gyro-period because instantaneous values of $\boldsymbol{v}_\perp$ and $\boldsymbol{B}$ are used in its computation, and these parameters do vary as the particle changes its position with time. The oscillations occur because the magnetic field is not uniform over a gyration, and the gyro-radius changes as particle move from the equatorial to the polar region. The average of these oscillating values over the gyro-period gives the first adiabatic invariant $J_1$ (shown by the black line), which is found to be constant with time only for the sixth-order Runge-Kutta method. From Fig. 6(a), it is evident that when the fourth-order Runge-Kutta method is used, $J_1$ is not constant with time. Therefore, the numerical dissipation in the fourth-order Runge-Kutta method makes this method inappropriate to study the complete motion of the charged particles in a static dipolar magnetic field.

The second adiabatic invariant is associated with the bounce motion between the magnetic mirror points. If

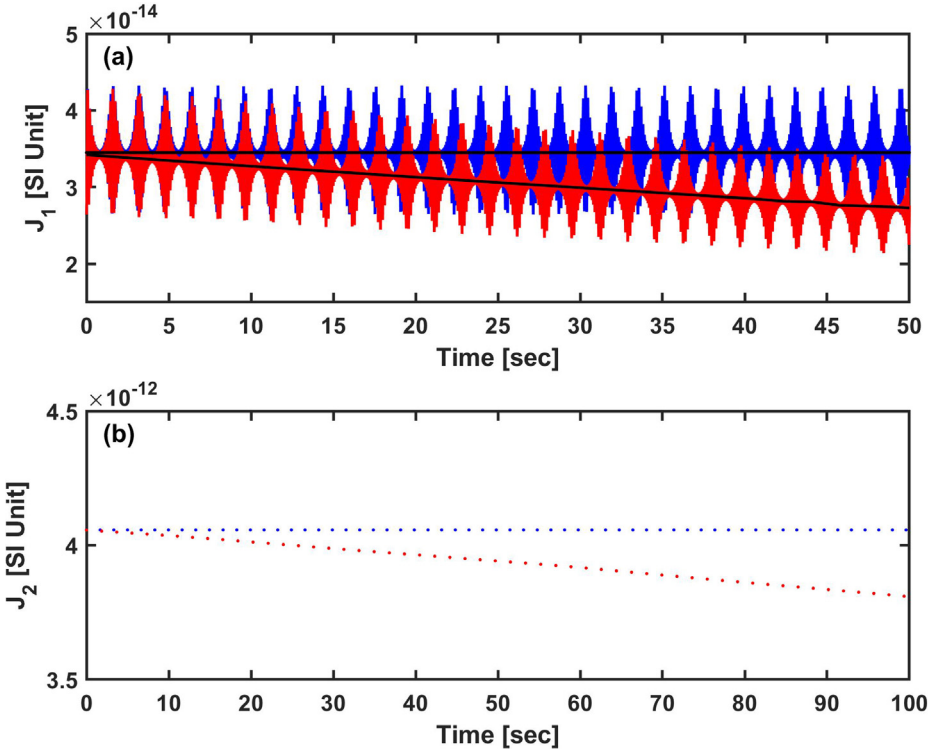


Fig. 6. (a) The instantaneous values of non-averaged (red and blue) and averaged $J_1$ (black) first adiabatic invariant as a function of time for 5 MeV proton initially placed at $L = 4$. The red and blue curves are obtained from the fourth- and sixth-order Runge-Kutta methods, respectively. (b) The second adiabatic invariant $J_2$ as a function of time, calculated from the parallel velocity of proton and averaged over the bounce period. Here, each dot represents the one bounce period over which the averaging is carried out to compute $J_2$. (For interpretation of the references to color in this figure legend, the reader is referred to the web version of this article.)

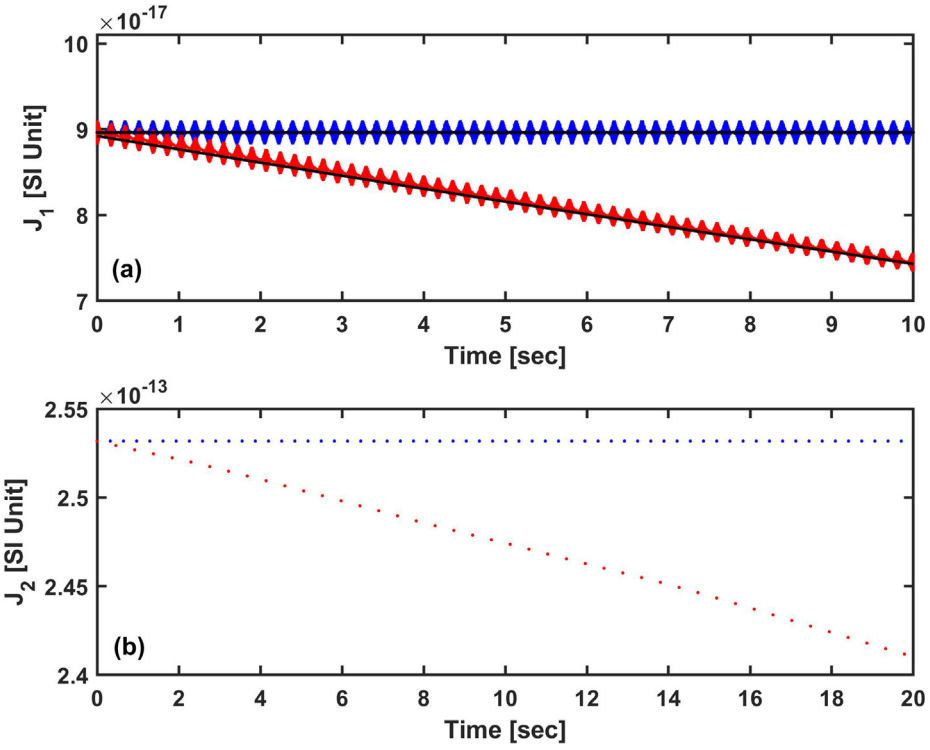


Fig. 7. (a) The instantaneous values of non-averaged (red and blue) and averaged $J_1$ (black) first adiabatic invariant as a function of time for 5 MeV electron initially placed at $L = 4$. The red and blue curves are obtained from the fourth- and sixth-order Runge-Kutta methods, respectively. (b) The second adiabatic invariant $J_2$ as a function of time, calculated from the parallel velocity of electron and averaged over the bounce period. Here, each dot represents the one bounce period over which the averaging is carried out to compute $J_2$. (For interpretation of the references to color in this figure legend, the reader is referred to the web version of this article.)

the azimuthal drift is small during a single bounce, the action variable associated with the bounce motion would be expected to be an invariant (Mahjouri, 1997). The expression for the second adiabatic invariant is given by,

$$J_2 = 2\int_{\lambda_{m1}}^{\lambda_{m2}} \gamma m_0 v_{\parallel} ds = 2\int_{\lambda_{m1}}^{\lambda_{m2}} \gamma m_0 v_{\parallel}^2 dt. \quad (9)$$

Here, $\lambda_{m1}$ and $\lambda_{m2}$ are magnetic latitudes of mirror points. The second adiabatic invariant is related to the field line's length between mirror points, which indicates that the field line length is constant as the particle drift in the azimuthal direction. Fig. 6(b) shows the variation of second adiabatic invariant $J_2$ as a function of time evaluated by integrating $\boldsymbol{v}_{\parallel}$ over one bounce period for proton of energy 5 MeV, and $L = 4$. The limits of integration are determined by the location of mirror points that are estimated from the simulation. It is evident in Fig. 6(b) that the second adiabatic invariant is also not conserved for the fourth-order Runge-Kutta method while it is conserved for the case of the sixth-order Runge-Kutta method.

Similar to Fig. 6, the variation of $J_1$ and $J_2$ for the electron of 5 MeV and $L = 4$ obtained from the simulation employing sixth-order and fourth-order Runge-Kutta methods are shown in Fig. 7. It may be noted that $J_1$ and $J_2$ are highly non-conserved for the fourth-order Runge-Kutta method. The third adiabatic invariant ($J_3$) is associated with the azimuthal drift motion of the mirror-trapped particles around the Earth. We have not compared $J_3$ because the charged particle cannot complete one drift motion due to higher numerical dissipation associated with the fourth-order Runge-Kutta method. However, $J_3$ can be computed from the simulation having employed the sixth-order Runge-Kutta method, and it is found to be conserved.

Thus, it is clear from Figs. 5–7 that the fourth-order Runge-Kutta method is not suitable to reproduce physically reliable trajectories of particles in the static dipolar magnetic field. The fourth-order Runge-Kutta method is sufficient to simulate the bounce motion of protons, one complete drift motion of proton of energy 10 MeV. However, three order smaller gyro-period of the electrons demands the numerical scheme with higher accuracy. Furthermore, the drift period increases for both lower energetic protons and electrons. In such a scenario, when we perform simulations for a longer time, numerical errors in the estimates of velocity and position of particles get integrated and subsequently enhanced. Therefore, one requires numerical schemes with higher numerical accuracy. We found that the sixth-order Runge-Kutta method is considerably stable and suitable to simulate both electron and proton trajectories of a wide range of energy and L-shell. For all the further simulation runs, we have used the sixth-order Runge-Kutta method.

## 4. Applications

We used the simulation model to obtain the trajectories of proton and electron of energy in the range of 5 keV to 250 MeV and L-shell 2–4. Their bounce and drift periods are estimated by tracking the variations of $\lambda$ and $\phi$ associated with their motions. The energy range for this comparison is chosen in such a way that all three adiabatic invariants are conserved. These simulated bounce ($\tau_b$) and drift ($\tau_d$) periods are validated by comparing them with their theoretical estimates which are available in the literature (Davidson, 1976; Orlova and Shprits, 2011). These expressions are not the exact form of the solution and based on the numerical fittings. Therefore, they deviate slightly (≈0.06%–5%) from their exact solution. The complete theoretical derivations of bounce and drift periods with their deviations are elaborated in Appendix B and C, respectively. We are using Eqs. (B.5) and (C.5) for the comparison with simulation results.

As mentioned earlier, the bounce period is calculated by tracking the variations in magnetic latitude, $\lambda$ with time. In one bounce, $\lambda$ can vary from $-90^\circ$ to $+90^\circ$ depending on the particle's mirror point latitude, $\lambda_m$. We have used one-dimensional Fast Fourier Transformation (FFT) on $\lambda$ to get the bounce motion period. The bounce period estimated from the simulation for protons and electrons of different energies placed at $L = 2$ (blue) and $L = 4$ (red) with their respective theoretical estimates (shown by "+" symbol) are shown in Fig. 8a and c, respectively. There is a good agreement between the bounce periods estimated from the simulation and theory for both proton and electron. The bounce period of the charged particle increases with their distance from the Earth. It is expected because the length of magnetic field line increases with L-shell, and hence particle needs to travel more distance along the field line. Further, we have computed the percentage difference ($\epsilon$) between the simulated and theoretical estimates of bounce periods for proton and electron, which is shown in Fig. 8(b), and (d), respectively. The percentage difference, $\epsilon$ is given by $\frac{|\tau_{theoretical}-\tau_{simulation}|\times 100}{\tau_{simulation}}$. The percentage difference between theoretical and simulated bounce periods is less than 5% and 1% for proton and electron, respectively, which is considerably small.

In the Earth's magnetosphere, a trapped charged particle performs drift motion around the Earth due to the gradient of magnetic field lines. Over one complete drift, azimuthal angle ($\phi$) varies from 0° to 360°. In the present simulation, the drift period is calculated by tracking the azimuthal angle variation, $\phi$for few drifts around the Earth. The drift period estimated from simulation are plotted as a function of energy for proton (Fig. 9a), and electron (Fig. 9c) placed at $L = 2$ (blue) and $L = 4$ (red) in Fig. 9. The respective theoretical estimates of drift periods are shown by the "+" symbol in Fig. 9a and c. It may be noted that unlike the bounce period, the drift period decreases with distance from the Earth. As we move away,

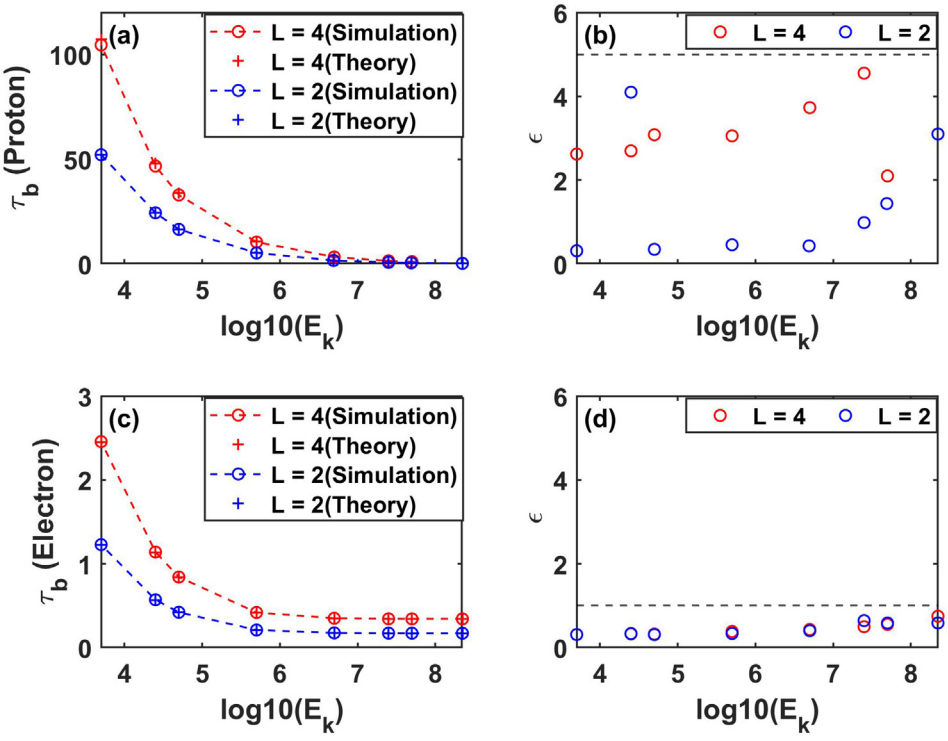


Fig. 8. The bounce period of (a) proton and (c) electron are shown as a function of energy for two different L-shells, $L = 4$ (red) and $L = 2$ (blue). The corresponding percentage difference between simulated and theoretical bounce periods ($\epsilon$) are depicted in panel-b for proton and in panel-d for electron. The maximum $\epsilon$ for proton and electron are ≈ 5% and 1%, respectively, which are shown by horizontal dash lines. (For interpretation of the references to color in this figure legend, the reader is referred to the web version of this article.)

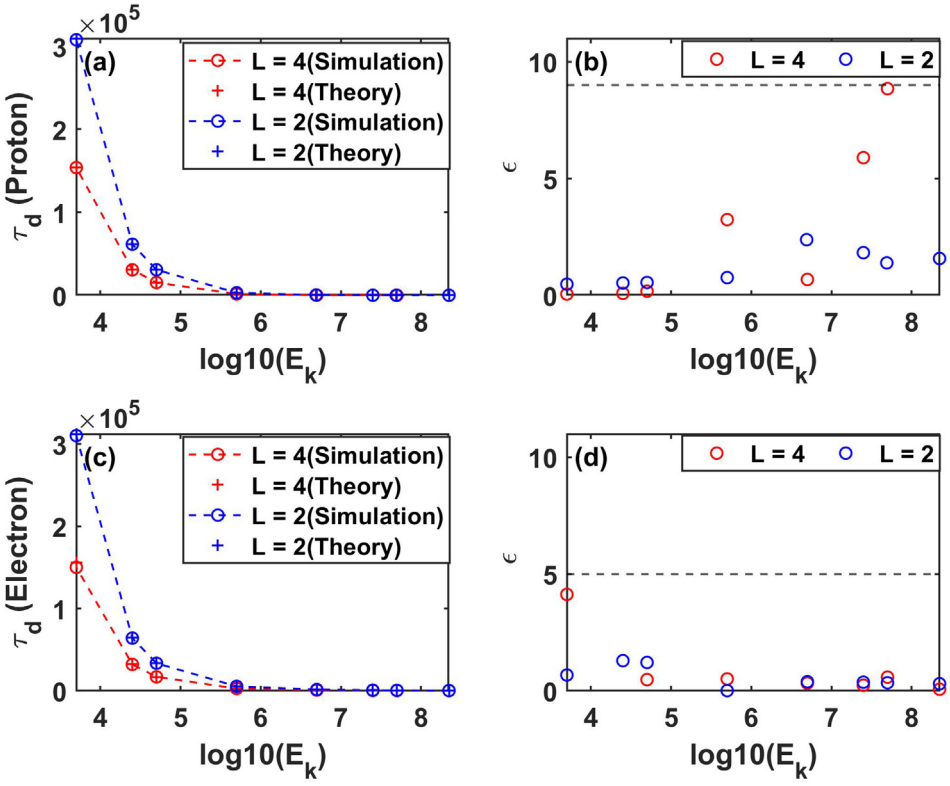


Fig. 9. The drift period of (a) proton and (c) electron are shown as a function of energy for two different L-shells, $L = 4$ (red) and $L = 2$ (blue). The corresponding percentage difference between simulated and theoretical bounce periods ($\epsilon$) are depicted in panel-b for proton and in panel-d for electron. The maximum $\epsilon$ for proton and electron are $\approx$ 9% and 5%, respectively, which are shown by horizontal dash lines. (For interpretation of the references to color in this figure legend, the reader is referred to the web version of this article.)

the magnetic flux density decreases, and the number of gyration in one drift reduces, which results in a faster azimuthal drift of the particle. The order of the drift period for electron and proton of given energy and L-shell are different because their azimuthal motion is a result of $\nabla B \times \mathbf{B}$ drift, which is charge and mass-dependent. The corresponding percentage difference between simulated and theoretical estimates of the drift period of proton and electron are shown in Fig. 9b and d, respectively. We noticed a good agreement between theoretical and simulated drift periods of proton and electron, and the corresponding percentage difference is less than 9% and 5%, respectively. Overall, this comparison implies that bounce and drift period's simulation results are in good agreement with their associated theoretical estimates.

## 5. Discussion

A magnetospheric trapped charged particle performs three types of periodic motion in the Earth's magnetosphere: gyration, bounce, and drift. We have developed a three-dimensional relativistic test particle simulation model by assuming the Earth's magnetic field in the dipolar configuration, which is a reasonable approximation for the inner magnetosphere. Since the particle is treated as a test particle, its motion does not affect the ambient magnetic field. Our primary focus is to check the suitability of the numerical scheme to trace the complete motion (gyro, bounce, and drift together) of the charged particle in the Earth's magnetic field. In many previous magnetospheric simulation studies, the particle motion is examined under guiding center approximation, which ignores the gyration and traces the trajectory of the only guiding center. Under this assumption, one can not see the effects of gyration on particle dynamics. In this simulation, a charged particle is allowed to gyrate, bounce, and drift in a self-consistent way. Therefore we can examine the effect of all three periodic motion on the particle dynamics. The simulation of drift motion of electrons (along with gyro and bounce motions) is computationally expensive and carried in very few previous studies using the guiding center approach (Sorathia et al., 2018). In such simulations, one needs an efficient numerical scheme so that the numerical dissipation is negligible, and simulations can be run for a long time to trace the drift motion of the charged particles. In the present simulation study, it is evident that the sixth-order Runge-Kutta method is appropriate to get the complete trajectories of both proton and electron.

We have noticed that the bounce and the drift period of both protons and electrons agree with the theory. The maximum deviation for the bounce and drift period of the proton is $\approx$ 5% and 9%, and for electron, they are $\approx$1%, and

5%, respectively. It may be noted that for proton, the error $\epsilon$ in the estimates of bounce and drift periods are slightly higher as compared to that of the electron. The theoretical expressions of the bounce and drift periods are summarised in Appendix B and C. These theoretical expressions of bounce and drift period are derived by averaging the particle motion over gyration. Since the gyro-radius of the electron is very small as compared to the proton, the electron gyrates very close to the magnetic field line, and the guiding center approximation used in theory is satisfied. However, in the proton case, the gyro-radius is larger, and the actual proton motion may deviate from their theoretical as they are based on the guiding center approximation. Thus, in the case of protons, the difference in the simulated and theoretical drift and bounce periods is higher than the electrons.

## 6. Conclusions

In the present paper, we have proposed an appropriate numerical scheme, which is capable of characterizing the all three motions (gyration, bounce, and azimuthal drift) of the charged particles of different energies that enter the Earth's magnetosphere and get trap along the magnetic field lines. The dipolar magnetic field configuration is assumed for the Earth, and the relativistic equation of motion for the charged particle is solved numerically to trace the trajectories of trapped charged particles of energy and L-shell in the range of 5 keV-250 MeV and $L = 2 - 6$, respectively. The efficiency of simulation model is tested using both fourth and sixth-order Runge-Kutta schemes by verifying the conservation of energy and adiabatic invariants. As an application of this model, we have simulated bounce and drift periods of protons and electrons of energy 5 keV to 250 MeV placed at $L = 2$ and 4 from the time variation of magnetic latitude ($\lambda$) and azimuthal angle ($\phi$), respectively. The theoretical expressions used to estimate the bounce and drift periods are elaborated in Appendix B and C. The primary outcomes of the study are as follows.

- A three-dimensional relativistic test particle simulation model is developed to examine the trajectories of charged particles trapped in the Earth's inner magnetosphere.
- Fourth-order Runge-Kutta method can simulate the bounce motion of the protons due to more numerical dissipation.
- Sixth-order Runge-Kutta method is required to simulate the motions of the electron and proton of energy 5 keV to 250 MeV placed at L = 2–6.
- The simulation results presented here are in good agreement with the theoretical estimates of the bounce and the drift periods.
- Our simulation validate the theoretical estimates of drift periods of both protons and electrons.
- Our simulation approach can be applied to the time-varying and non-analytical form of magnetic field configuration in the Earth's inner magnetosphere in future studies.

## Declaration of Competing Interest

The authors declare that they have no known competing financial interests or personal relationships that could have appeared to influence the work reported in this paper.

## Acknowledgments

The model computations were partly performed on the High-Performance Computing System at the Indian Institute of Geomagnetism.

## Appendix A. Runge-Kutta method

The function with initial condition $y(t_0) = y_0$ is specified as follows,

$$\dot{y} = f(t, y). \tag{A.1}$$

Here, $y$ is an unknown function of time $t$, which has to be solved using Runge-Kutta method. The rate at which this function changes with time is defined by $f(t, y)$. Since the initial condition is known, the value of the unknown function ($y$) for next time step can be computed as,

$$\begin{aligned} y_{n+1} &= y_n + \tfrac{h}{5}\left[\tfrac{16k_1}{27} + \tfrac{6656k_3}{2565} + \tfrac{28561k_4}{11286} - \tfrac{9k_5}{10} + \tfrac{2k_6}{11}\right], \\ t_{n+1} &= t_n + h. \end{aligned} \tag{A.2}$$

Here, $h$ is the positive step size and $n$ is the limit up to which unknown function has to be solved. The coefficients $k_1 - k_6$ are obtained from function $f(t, y)$ using following expressions,

$$\begin{aligned} k_1 &= f(t_n, y_n), \\ k_2 &= f(t_n + \tfrac{h}{4}, y_n + \tfrac{hk_1}{4}), \\ k_3 &= f(t_n + \tfrac{3h}{8}, y_n + \tfrac{3h}{32}(k_1 + 3k_2)), \\ k_4 &= f(t_n + \tfrac{12h}{13}, y_n + \tfrac{12h}{2197}(161k_1 - 600k_2 + 608k_3)), \\ k_5 &= f(t_n + h, y_n + \tfrac{h}{4104}(8341k_1 - 32832k_2 + 29440k_3 - 845k_4)), \\ k_6 &= f(t_n + \tfrac{h}{2}, y_n + h(-\tfrac{8}{27}k_1 + 2k_2 - \tfrac{3544}{2565}k_3 + \tfrac{1859}{4104}k_4 + \tfrac{11}{40}k_5)). \end{aligned} \tag{A.3}$$

In our simulation model, $[\boldsymbol{v_x}, \boldsymbol{v_y}, \boldsymbol{v_z}]$ and $[\boldsymbol{x}, \boldsymbol{y}, \boldsymbol{z}]$ are unknown function of time. The rate from which these function changes are defined as right hand side of in Eqs. (1) and (2). The equations are first solved for velocity and then for position. In similar way, fourth-order Runge-Kutta method can be employed with $y_{n+1}$ as,

$$y_{n+1} = y_n + \frac{h}{6}[k_1 + 2k_2 + 2k_3 + k_4]. \tag{A.4}$$

$$\begin{aligned} k_1 &= f(t_n, y_n), \\ k_2 &= f(t_n + \tfrac{h}{2}, y_n + \tfrac{hk_1}{2}), \\ k_3 &= f(t_n + \tfrac{h}{2}, y_n + \tfrac{hk_2}{2}), \\ k_4 &= f(t_n + h, y_n + hk_3). \end{aligned} \tag{A.5}$$

## Appendix B. Bounce period

The bounce period of a charged particle can be calculated by integrating the $ds/v_\parallel$ over the full bounce path along magnetic field line.

$$\tau_b = 4\int_{\lambda_m}^{\pi/2} \frac{ds}{v_\parallel} = 4\int_{\lambda_m}^{\pi/2} \frac{ds}{d\lambda}\frac{d\lambda}{v_\parallel}. \tag{B.1}$$

Here, $ds$ is arc element along magnetic field line and $\lambda$ is magnetic latitude. The subscript "$m$" denotes "mirror point". After inserting the expression of $v_\parallel$ and change of arc element of field line with magnetic latitude ($ds/v_\parallel$), we obtained bounce period as,

$$\begin{aligned} \tau_b &= 4\frac{r_{eq}}{v}\int_{\lambda_m}^{\pi/2} \frac{sin\lambda(1+3cos^2\lambda)^{1/2}}{\left[1 - sin^2\alpha_{eq}\frac{(1+3cos^2\lambda)^{1/2}}{sin^6\lambda}\right]^{1/2}} d\lambda \\ &= 4\frac{r_{eq}}{v}T(y). \end{aligned} \tag{B.2}$$

Here, $y \equiv sin\alpha_{eq}$. The integral has a singularity at the mirror points which do not allow to solve it analytically. Therefore, the integral has been evaluated numerically to find the exact expression of the bounce period. The integral $T(y)$ depends on the equatorial pitch angle($\alpha_{eq}$) and solved over $\lambda$. In order to find the numerical solution, one has to solve the integral for different values of $\lambda_m$ varying from 0 to 90° at a fixed pitch angle. The numerical solution of the integral $T(y)$ can be treated as an exact solution and can be approximated with numerical fitting for $T(y)$ as a function of $y$.

Different approximations were found empirically three decades ago (Davidson, 1976; Hamlin et al., 1961). Recently, Orlova and Shprits (2011) proposed the following approximations for the integral $T(y)$,

$$\begin{aligned} T_1(y) &\approx 1.30 - 0.56y, \\ T_2(y) &\approx 1.38 - 0.32(y + y^{1/2}), \\ T_3(y) &\approx 1.3802 - 0.6397y^{3/4}, \\ T_4(y) &\approx 1.38 + 0.055y^{1/3} - 0.32y^{1/2} - 0.037y^{2/3} \\ &\quad -0.394y + 0.056y^{4/3} \end{aligned} \tag{B.3}$$

All these approximations have a deviation from an exact solution which is measured as an absolute percentage deviation defined as,

$$\delta = \frac{|\,\tau_{approx}(y) - \tau_{exact}(y)\,|}{T_{exact}(y)}100\%. \tag{B.4}$$

All approximations $T_1(y), T_2(y), T_3(y)$, and $T_4(y)$ are compared with the exact solution in Fig. B.10. The red line in panels (a) to (d) of this figure shows the exact solution of integral T(y) and blue line is the approximated results. The absolute percentage deviation ($\delta$) for the approximation $T_1(y), T_2(y), T_3(y)$, and $T_4(y)$ is shown in panels (e)-(h) of Fig. B.10. The maximum value of deviation ($\delta_{max}$) shows that the approximation $T_1(y)$ is less accurate. The parametrization of approximation $T_4(y)$ was formed as linear combination of the most important terms and is considerably more accurate. Here, we have used the approximation $T_3(y)$ to estimate the theoretical expression because its maximum deviation is 0.5% and has only three terms. Using the approximation $T_3(y)$, the expression for bounce period can be written as,

$$\tau_b = 0.117L\frac{c}{v}[1 - 0.4635(sin\alpha_{eq})^{3/4}]. \tag{B.5}$$

Here, $R_e$ is the radius of Earth and $L$ is the distance from the center of the dipole to the equatorial crossing of the field line in terms of $R_e$. In order to include relativistic effect in this expression, the velocity $\mathbf{v}$ is calculated from the energy of particle using relativistic transformation defined in Eq. (3). It may be noted that when we compute $\tau_b$ from Eq. (B.1), the gyration of particle is not considered. Also solving Eq. (B.2) by using approximations forms given in Eq. (B.3) can introduce some errors in the estimates of $\tau_b$.

## Appendix C. Drift period

Drift period of a charged particle can be calculated by the rate of change of azimuth angle ($\phi$) over a bounce,

$$< \frac{d\phi}{dt} > = \frac{\Delta\phi}{\tau_b} = \frac{4}{\tau_b}\int_{\lambda_m}^{\pi/2} \frac{v_\perp(\lambda)}{R_0 cos^3\lambda}\frac{ds}{d\lambda}\frac{d\lambda}{v_\parallel}. \tag{C.1}$$

Using the expression of $v_\parallel, v_\perp$ and $ds/d\lambda$, we can get change in azimuth angle as,

$$\begin{aligned} < \frac{d\phi}{dt} > &= \frac{4}{\tau_b}\frac{3m_0vR_0^2}{qB_0R_e^3}\int_{\lambda_m}^{\pi/2} \frac{cos^3\lambda(1+3sin^2\lambda)[1 - \frac{v^2}{2}\frac{(1+3sin^2\lambda)^{1/2}}{cos^6\lambda}])}{(1+3sin^2\lambda)^{3/2}[1 - y^2\frac{(1+3sin^2\lambda)^{1/2}}{cos^6\lambda}]^{1/2}} d\lambda \\ &= \frac{4}{\tau_b}\frac{3m_0v(LR_e)^2}{qB_0R_e^3}E(y). \end{aligned} \tag{C.2}$$

Time taken for a complete rotation of longitude ($2\pi$) will be drift period,

$$\tau_d = \frac{2\pi}{< \frac{d\phi}{dt} >} = \frac{2\pi qB_0R_e^2}{3Lm_0v^2}\frac{T(y)}{E(y)} = \frac{2\pi qB_0R_e^2}{3Lm_0v^2}D(y). \tag{C.3}$$

Again, similar to $T(y)$, integral $E(y)$ is also singular at mirror point and needs to solve numerically with the varying value of $\lambda$ which will be treated as exact solution. This integral can also be approximated with numerical fitting for integral $D(y)$ with $y$. Past approximations for integral $D(y)$ includes Hamlin et al. (1961),

$$\begin{aligned} D_1(y) &\approx 0.35 + 0.154y, \\ D_2(y) &\approx 1/3(1 - 0.3333(sin\alpha_{eq})^{0.62}). \end{aligned} \tag{C.4}$$

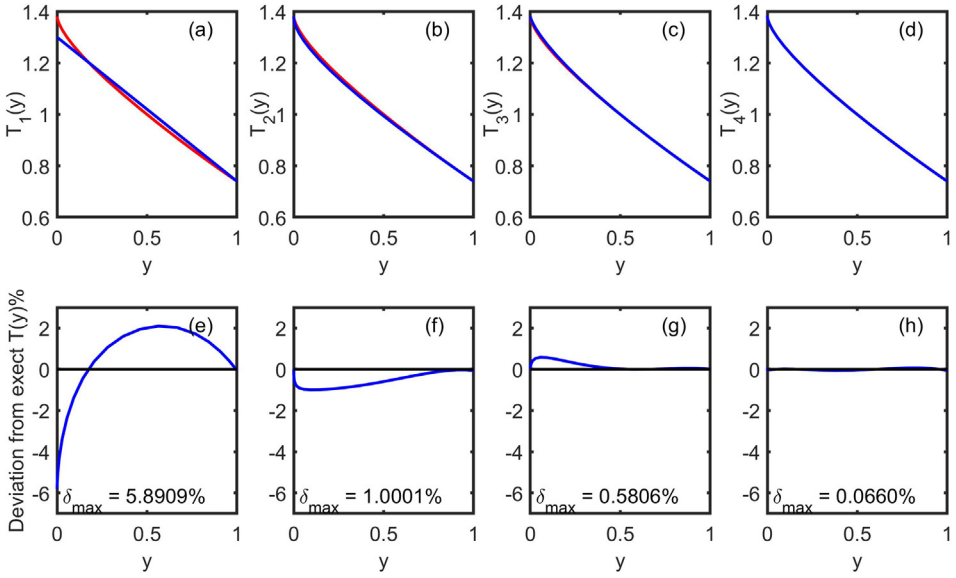


Fig. B.10. Comparison of approximation $T_1(y), T_2(y), T_3(y)$, and $T_4(y)$ with the exact solution. Panels (a)-(d) show the exact solution of $T(y)$ (plotted with red color) and all approximations (plotted with blue) as a function of $y$. Panels (e)-(f) show the percentage deviation(plotted with blue) of approximations with exact solution. The maximum percentage deviation($\delta_{max}$) for each approximation is given in respective subplots. Here, black line represents the approximation with zero deviation. (For interpretation of the references to color in this figure legend, the reader is referred to the web version of this article.)

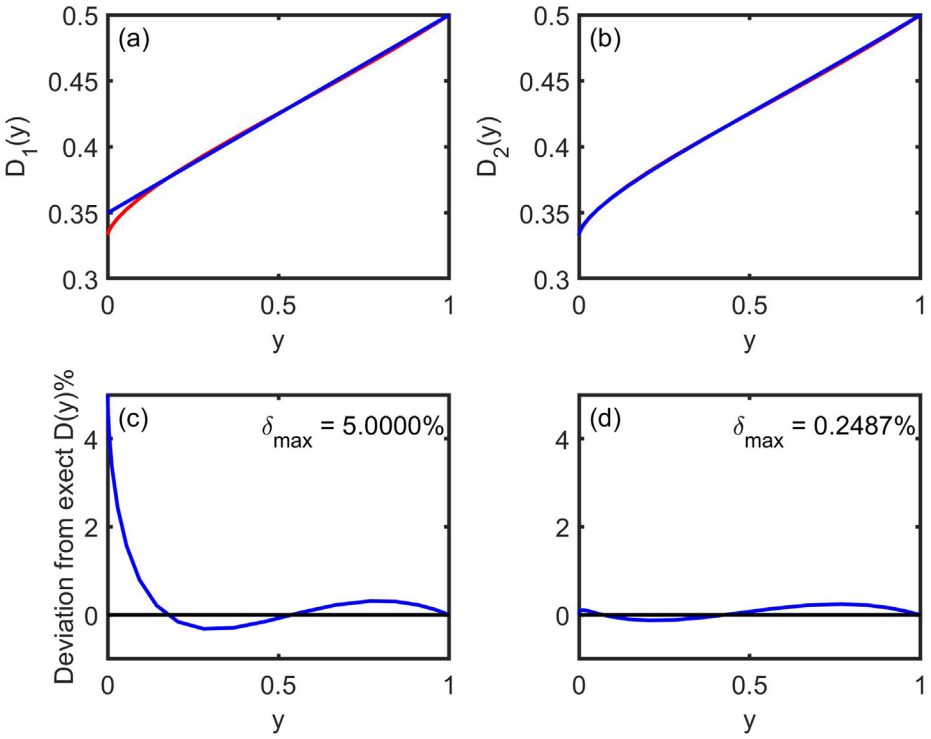


Fig. C.11. Comparison of approximation $D_1(y)$ and $D_2(y)$ with exact solution. (a) and (b) shows the exact solution of $D(y)$ (plotted with red color) and approximated (plotted with blue) as a function of $y$. (c) and (d) shows the percentage deviation (plotted with blue) of approximations with the exact solution. The maximum percentage deviation ($\delta_{max}$) for each approximation is written. The black line at zero represents the approximation with zero deviation. (For interpretation of the references to color in this figure legend, the reader is referred to the web version of this article.)

The approximations $D_1(y)$ and $D_2(y)$ as a function of "$y$" are shown Fig. C.11. The red curve of Fig. C.11(a) and (b) represents the exact solution of integral $D(y)$ while blue represents the approximated $D_1(y)$ and $D_2(y)$. The absolute percentage deviation of these approximations from the exact solution is shown in Fig. C.11(c) and (d). The maximum percentage deviation shows that $D_1(y)$ is less accurate. Using approximation $D_2(y)$, the expression for drift period can be written as,

$$\tau_d = \frac{2\pi q B_0 R_e^3}{mv^2}\frac{1}{LR_e}\left[1-\frac{1}{3}(sin\alpha_{eq})^{0.62}\right]. \quad \text{(C.5)}$$

## References


A.E. Antonova, Y.G., Kropotkin, A., 2003. Effects in the radiation belts caused by the second adiabatic invariant violation in the presence of dayside off-equatorial magnetic field minima. Adv. Space Res. 31, 223–1228. https://doi.org/10.1016/S0273-1177(02)00934-1.

Baumjohann, W., Treumann, R., 2012. Basic space. Plasma Phys. https://doi.org/10.1142/P850.

Birmingham, T., Northrop, T., Fälthammar, C.G., 1967. Charged particle diffusion by violation of the third adiabatic invariant. Phys. Fluids 10, 2389–2398. https://doi.org/10.1063/1.1762048.

Bittencourt, J., 2011. Fundamental of Plasma Physics. Springer. https://doi.org/10.1007/978-1-4757-4030-1.

Chen, F., 1984. Introduction to Plasma Physics and Controlled Fusion vol. 1, Springer. https://doi.org/10.1007/978-3-319-22309-4.

Davidson, G., 1976. An improved empirical description of the bounce motion of trapped particles. J. Geophy. Res. Space Phys. 81, 4029–4030. https://doi.org/10.1029/JA081i022p04029.

Delcourt, D., Sauvaud, J., Pedersen, A., 1990. Dynamics of single-particle orbits during substorm expansion phase. J. Geophy. Res. Space Phys. 95, 20853–20865. https://doi.org/10.1029/JA095iA12p20853.

Ebihara, Y., Miyoshi, Y., 2011. Dynamic inner magnetosphere: A tutorial and recent advances, pp. 145–187. https://doi.org/10.1007/978-94-007-0501-2-9.

Elkington, S.R., Hudson, M.K., Chan, A.A., 2003. Resonant acceleration and diffusion of outer zone electrons in an asymmetric geomagnetic field. J. Geophy. Res. Space Phys. 108. https://doi.org/10.1029/2001JA009202.

Engel, M., Kress, B., Hudson, M., Selesnick, R., 2015. Simulations of inner radiation belt proton loss during geomagnetic storms. J. Geophy. Res. Space Phys. 120, 9323–9333. https://doi.org/10.1002/2015JA021568.

Griffiths, D.J., 2005. Introduction to electrodynamics. AAPT.

Hamlin, D.A., Karplus, R., Vik, R., Watson, K., 1961. Mirror and azimuthal drift frequencies for geomagnetically trapped particles. J. Geophy. Res. Space Phys. 66, 1–4. https://doi.org/10.1029/JZ066i001p00001.

Hones, J., Edward, W., 1963. Motions of charged particles trapped in the earth's magnetosphere. J. Geophys. Res. 1896–1977 (68), 1209–1219. https://doi.org/10.1029/JZ068i005p01209.

Hudson, M., Jaynes, A., Kress, B., Li, Z., Patel, M., Shen, X.C., Thaller, S., Wiltberger, M., Wygant, J., 2017. Simulated prompt acceleration of multi-mev electrons by the 17 March 2015 interplanetary shock. J. Geophy. Res. Space Phys. 122, 10–036. https://doi.org/10.1002/2017JA024445.

Katoh, Y., Omura, Y., 2004. Acceleration of relativistic electrons due to resonant scattering by whistler mode waves generated by temperature anisotropy in the inner magnetosphere. J. Geophy. Res. Space Phys. 109. https://doi.org/10.1029/2004JA010654.

Kellogg, P.J., 1959. Van allen radiation of solar origin. Nature 183. https://doi.org/10.1038/1831295a0.

Luther, H., 1968. An explicit sixth-order Runge-Kutta formula. Math. Comput. 22, 434–436. https://doi.org/10.1090/S0025-5718-68-99876-1.

Mahjouri, M., 1997. Simulation of charged particle motion in jupiter's magnetosphere. Acta Phys. Polonica-Ser. A Gen. Phys. 92, S21.

Millan, R., Baker, D., 2012. Acceleration of particles to high energies in earth's radiation belts. Space Sci. Rev. 173, 103–131. https://doi.org/10.1007/s11214-012-9941.

Mozer, F., Bale, S., Bonnell, J., Chaston, C., Roth, I., Wygant, J., 2013. Megavolt parallel potentials arising from double-layer streams in the earth's outer radiation belt. Phys. Rev. Lett. 111, 235002. https://doi.org/10.1103/PhysRevLett.111.235002.

Mukherjee, G., Rajaram, R., 1981. Motion of charged particles in the magnetosphere. Astrophys. Space Sci. 74, 287–301. https://doi.org/10.1007/BF00656440.

Northrop, T.G., Teller, E., 1960. Stability of the adiabatic motion of charged particles in the earth's field. Phys. Rev. 117, 215. https://doi.org/10.1103/PhysRev.117.215.

Orlova, K., Shprits, Y., 2011. On the bounce-averaging of scattering rates and the calculation of bounce period. Phys. Plasmas 18, 092904. https://doi.org/10.1063/1.3638137.

Ozaki, M., Miyoshi, Y., Shiokawa, K., Hosokawa, K., Oyama, S.i., Kataoka, R., Ebihara, Y., Ogawa, Y., Kasahara, Y., Yagitani, S., et al., 2019. Visualization of rapid electron precipitation via chorus element wave–particle interactions. Nat. Commun. 10, 257. https://doi.org/10.1038/s41467-018-07996-z.

Öztürk, M.K., 2012. Trajectories of charged particles trapped in earth's magnetic field. Am. J. Phys. 80. https://doi.org/10.1119/1.3684537.

Portero, L., Arrarás, A., Jorge, J., 2012. Variable step-size fractional step Runge–Kutta methods for time-dependent partial differential equations. Appl. Numer. Math. 62, 1463–1476. https://doi.org/10.1016/j.apnum.2012.06.015.

Reeves, G., Spence, H.E., Henderson, M., Morley, S., Friedel, R., Funsten, H., Baker, D., Kanekal, S., Blake, J., Fennell, J., et al., 2013. Electron acceleration in the heart of the van allen radiation belts. Science 341, 991–994. https://doi.org/10.1126/science.1237743.

Sorathia, K.A., Ukhorskiy, A.Y., Merkin, V.G., Fennell, J.F., Claudepierre, S.G., 2018. Modeling the depletion and recovery of the outer radiation belt during a geomagnetic storm: Combined mhd and test particle simulations. J. Geophy. Res. Space Phys. 123, 5590–5609. https://doi.org/10.1029/2018JA025506.

Tobita, M., Omura, Y., 2018. Nonlinear dynamics of resonant electrons interacting with coherent langmuir waves. Phys. Plasmas 25, 032105. https://doi.org/10.1063/1.5018084.

Ukhorskiy, A.Y., Sitnov, M.I., 2008. Radial transport in the outer radiation belt due to global magnetospheric compressions. J. Atmos. Solar-Terrestrial Phys. 70, 1714–1726. https://doi.org/10.1016/j.jastp.2008.07.018.

Walt, M., 2005. Introduction to Geomagnetically Trapped Radiation vol. 1. https://doi.org/10.1017/CBO9780511524981.

Williams, D.J., 1971. Charged particles trapped in the earth's magnetic field 15, 137–218. https://doi.org/10.1016/S0065-2687(08)60302-7.

Yugo, H., Iyemori, T., 2001. Symplectic integration: A new approach to tracing charged particle motion in the geomagnetic field. J. Geophy. Res. Space Phys. 106, 26075–26079. https://doi.org/10.1029/2000JA000424.